Water Supply

IWA PUBLISHING

Water Supply Vol 22 No 3, 3307 doi: 10.2166/ws.2021.397

Application of meteorological element combination-driven SWAT model based on meteorological datasets in alpine basin

Pengfei Gu [a,b], Yongxiang Wu[b], Guodong Liu[a,*], Chengcheng Xia[a], Gaoxu Wang[b], Jing Xia[a], Ke Chen[a], Xiaohua Huang[a] and Daiyuan Li[b]

[a] State Key Laboratory of Hydraulics and Mountain River Engineering, College of Water Resource & Hydropower, Sichuan University, Chengdu 610065, Sichuan Province, China
[b] State Key Laboratory of Hydrology-Water Resources and Hydraulic Engineering, Nanjing Hydraulic Research Institute, 225 Guangzhou Road, Nanjing 210029, China
*Corresponding author. E-mail: liugd988@163.com

PG, 0000-0002-2147-8690

ABSTRACT

Thus far, reanalysis-based meteorological products have drawn little attention to the influence of meteorological elements of products on hydrological modeling. This study aims to evaluate the hydrological application potential of the precipitation, temperature, and solar radiation of the China Meteorological Assimilation Driving Datasets for the Soil and Water Assessment Tool (SWAT) model (CMADS) and Climate Forecast System Reanalysis (CFSR) in an alpine basin. The precipitation, temperature, and solar radiation of the gauge-observed meteorological dataset (GD), CFSR, and CMADS were cross-combined, and 20 scenarios were constructed to drive the SWAT model. From the comprehensive comparisons of all scenarios, we drew the following conclusions: (1) among the three meteorological elements, precipitation has the greatest impact on the simulation results, and using GD precipitation from sparse stations yielded better performance than CMADS and CFSR; (2) although the SWAT modeling driven by CMADS and CFSR performed poorly, with CMADS underestimation and CFSR overestimation, the temperature and solar radiation of CMADS and CFSR can be an alternative data source for streamflow simulation; (3) models using GD precipitation, CFSR temperature, and CFSR solar radiation as input yielded the best performance in streamflow simulation, suggesting that these data sources can be applied to this data-scarce alpine region.

Key words: alpine basin, CFSR, CMADS, combination, SWAT

HIGHLIGHTS

- The performance of SWAT driven by a combination of multi-meteorological elements is evaluated for the first time in the YRSR.
- Precipitation, temperature, and solar radiation of two reanalysis-based meteorological products were tested in the alpine basin.
- Using the GD precipitation, CFSR temperature, and CFSR solar radiation drove SWAT to yield the best performance in the YRSR.

1. INTRODUCTION

Meteorological data are necessary to drive hydrological models, and the spatial and temporal accuracy of data directly affects the model simulation quality (Eini *et al.* 2019; Wang *et al.* 2020). Unfortunately, meteorological stations are sparse in alpine basins with complex topographies and harsh climates (Bhatta *et al.* 2019), and point-based monitoring ranges are limited (Duan *et al.* 2019). However, alpine basins are essential to the conservation of water resources, such as the Tibetan Plateau known as Asia's water towers (Immerzeel *et al.* 2010). Therefore, in alpine basins, it is necessary to increase the network density of meteorological stations (finances permitting) or explore alternative meteorological data sources.

Many reanalysis-based meteorological products have been developed and released to the public (Saha *et al.* 2010, 2014; Yatagai *et al.* 2012; Meng *et al.* 2016), providing an opportunity for hydrological model research in basins where meteorological data are scarce (Famiglietti *et al.* 2015; Sun *et al.* 2018). These products have the advantages of extensive coverage, high spatiotemporal resolution, and continuous observation (Bajracharya *et al.* 2015; Prakash *et al.* 2016) and have been widely applied in hydrological studies in many regions (Saha *et al.* 2010; Fuka *et al.* 2014; De Almeida Bressiani *et al.* 2015;

Auerbach *et al.* 2016; Meng *et al.* 2016, 2019; Wang *et al.* 2020). However, most of these studies have focused on the applicability of products to basins or hydrological models (Fuka *et al.* 2014; Auerbach *et al.* 2016; Liu *et al.* 2018) or discussing the application potential of the precipitation elements of products in hydrological modeling (Awange *et al.* 2019; Guo *et al.* 2019; Wang *et al.* 2020). If product-driven hydrological models yield unsatisfactory performance, the products are considered inapplicable in that catchment. However, these products contain multiple meteorological elements, such as CFSR contains almost all the meteorological elements required by hydrological modeling, including precipitation, temperature, solar radiation, wind speed, and relative humidity. Poor product performance does not prove that the various meteorological elements of the products perform poorly.

Several studies (Duan *et al.* 2019; Mm *et al.* 2019) demonstrated that hydrological models driven by CFSR yielded unsatisfactory performance in Ethiopia, but hydrological models driven by the combination of the Climate Hazards Group InfraRed Precipitation with Station data (CHIRPS) precipitation and CFSR temperature achieved good simulation results (Duan *et al.* 2019). In the Cau River basin of Vietnam, Dao *et al.* (2021) reported that the precipitation quality of CMADS and CFSR is poor, but better temperature quality is a good potential data source. Although many studies (Villarini *et al.* 2009; Strauch *et al.* 2012; Monteiro *et al.* 2016; Duan *et al.* 2019) have shown that precipitation is the key factor affecting hydrological-runoff simulation, it is not enough to study the influence of precipitation on hydrological-runoff simulation in alpine basins with low temperatures and strong radiation. Therefore, it is necessary to analyze the application potential of each meteorological element of meteorological products in hydrological-runoff simulations, especially in alpine basins.

The overall objective of this study was to evaluate the hydrological application potential of the precipitation, temperature, and solar radiation of CMADS and CFSR in the Yellow River Source Region (YRSR). To achieve this objective, the present study involved the following: (1) the applicability of the precipitation, temperature, and solar radiation of CMADS and CFSR was systematically evaluated using multiple indicators based on the appropriate time scale in the study area; (2) Using multi-meteorological datasets [gauge-observed meteorological dataset (GD), CMADS, and CFSR], precipitation, temperature, and solar radiation were cross-combined, and 20 scenarios (Table 3) were constructed to drive the SWAT model. To the best of our knowledge, the influence of the combination of precipitation, temperature, and solar radiation from a multi-source meteorological dataset on hydrological models in alpine basins has not been considered in previous studies.

2. MATERIALS AND METHODS

2.1. Research area

The YRSR is the basin above the Tangnaihai hydrological station (Gao *et al.* 2018a), and is considered the 'water tower' of the Yellow River, accounting for only 15% of the entire basin (Yuan *et al.* 2018) but contributes 35% of the water volume in the basin (Hu *et al.* 2011). The YRSR belongs to a typical Qinghai-Tibet Plateau climate (Xu & He 2006; Yuan *et al.* 2018), with strong radiation levels, low temperatures, and meteorological data scarcity. Rainfall is predominately concentrated in the flood season (June–October), accounting for approximately 75% of the annual precipitation, and snowfall is primarily concentrated from September to May (Hu *et al.* 2011). The mean basin annual precipitation for many years (2008–2012) is approximately 566.96 mm (Figure 3). Rainfall-runoff is the predominant runoff pattern in the YRSR, accounting for 95.9% of the total runoff (Liu & Chang 2005). Based on the measured temperature from gauge stations for the period 2008–2012, the annual average daily maximum temperature is 9.53 °C, and the minimum temperature is −4.99 °C (Figure 3).

2.2. Data

2.2.1. Meteorological datasets

Three types of meteorological datasets, namely, the GD, CMADS, and CFSR, were selected for this study.

The GD was derived from the daily surface meteorological data of the China Meteorological Data Network (version 3.0) (http://data.cma.cn/), including precipitation, temperature, relative humidity, and wind speed. There is only one Maduo station northwest of the basin (Figure 1). Therefore, two weather stations (Nuomuhong (NMH) and Qumalai (QML)) located outside the catchment were selected and used as weather stations in the 7th and 8th sub-basins (distance: D(NMH-7)<D(MD-7), D(QML-8)<D(MD-8)), respectively.

The CMADS was established using the China Meteorological Administration atmospheric assimilation system technology and multiple scientific methods, and it covers all of East Asia (0–65° N, 60–60° E), providing all the meteorological elements needed for the SWAT model from 2008 to 2016 (Meng *et al.* 2018). The present study adopted version 1.1 of CMADS at a spatial resolution of 25×25 km (http://westdc.westgis.ac.cn/), and a total of 198 sites were selected based on the research

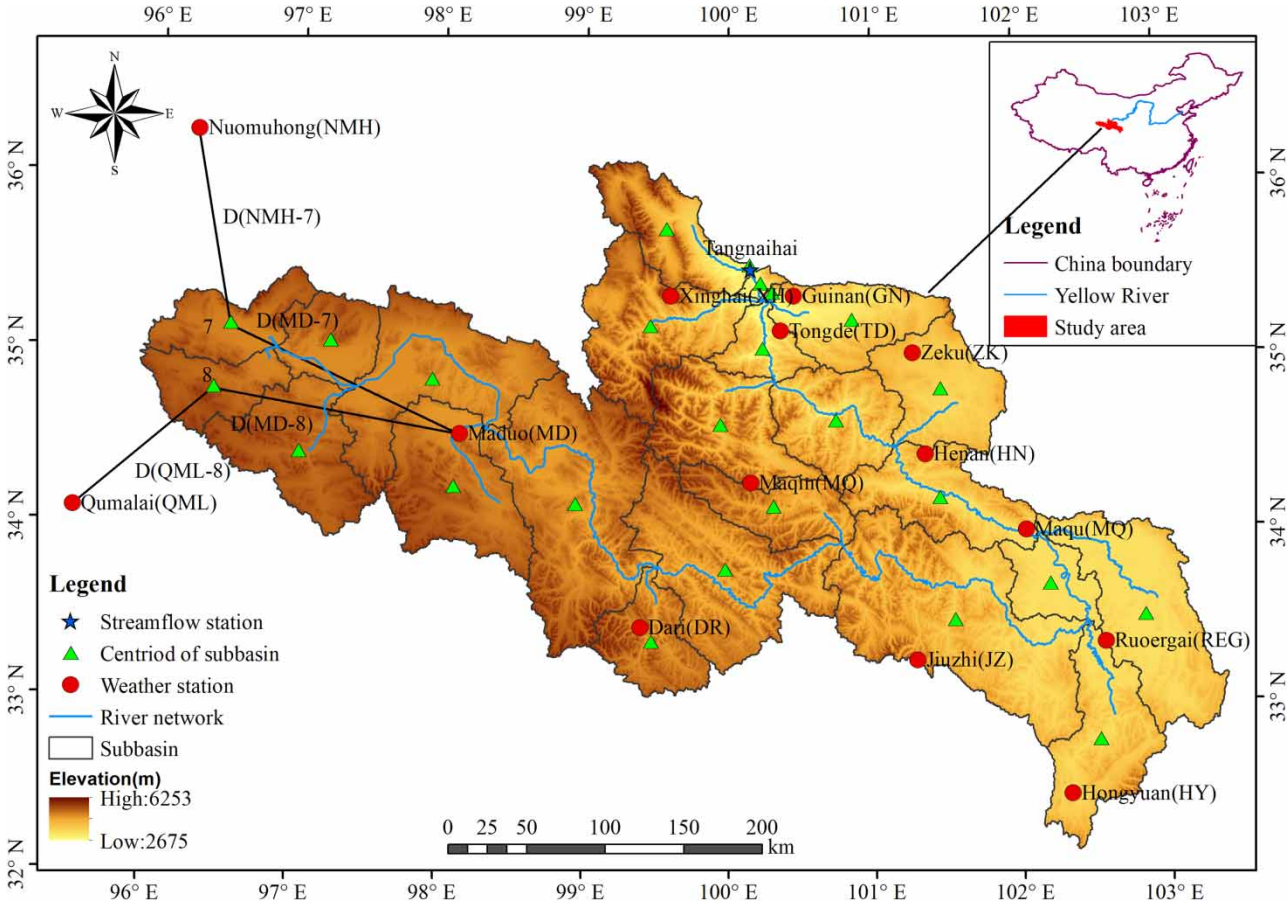

Figure 1 | Map of the YRSR.

area. The CFSR provided by the National Centers for Environmental Prediction (NCEP) was completed over 36 years (1979–2014) (https://globalweather.tamu.edu/). It is an interpolation dataset on a 38×38 km^2 grid that integrates surface meteorological gauge data and satellite remote sensing data using assimilation technology and advanced atmospheric, oceanic, and land components (Saha *et al.* 2014). A total of 122 sites were selected in the study area.

2.2.2. Other data

In addition to meteorological data, the following data are needed for model construction and verification: (1) Digital Elevation Model (DEM) data were derived from SRTM_DEM data with a 90-m spatial resolution provided by the Geospatial Data Cloud (http://www.gscloud.cn/); (2) Land use data were derived from the Chinese Academy of Sciences Resource and Environmental Science Data Center, with a resolution of 1 km (http://www.resdc.cn/); (3) Soil data were derived from the Harmonized World Soil Database (HWSD) constructed by Food and Agriculture Organization of the United Nations (FAO) and International Institute for Applied Systems Analysis (IIASA), with a resolution of 1 km (http://westdc.westgis.ac.cn/); (4) Streamflow data at the Tangnaihai station from 1 January 2008 to 31 December 2012 were collected from the Nanjing Hydraulic Research Institute, China. To ensure coordinate consistency and spatial data projections, we set the coordinate projection system of the DEM, land use data, and soil data to that of WGS_1984_Albers, with a central longitude of 100° E and standard latitude (north latitude) of $\emptyset_1$=33.5°, $\emptyset_2$=38°.

2.3. Methods

There are two main parts of this paper. The first part (precipitation, temperature, and solar radiation data evaluation) aims to evaluate the applicability of precipitation, temperature, and solar radiation of CFSR and CMADS. The second part (streamflow simulation) uses the meteorological elements of precipitation, temperature, and solar radiation to cross-combine drive

SWAT models to evaluate the accuracy and application potential in streamflow simulation. The analysis process used in the present study is shown in Figure 2.

2.3.1. Accuracy evaluation method for re-analysis datasets

To quantitatively evaluate the accuracy of precipitation and temperature from re-analysis datasets, three statistical metrics, including the root mean square error (RMSE), percent bias (PBIAS), and correlation coefficient (CC), were selected at two temporal scales of month and year. The RMSE was used to measure the deviation of the evaluated data compared with that of the gauged data (Eini *et al.* 2019). The PBIAS denotes the absolute error between the evaluated and gauged data (Yuan *et al.* 2018). Positive (negative) values indicate that the evaluated data were overestimated (underestimated). The CC exhibited a linear correlation between the evaluated and gauged data (Eini *et al.* 2019). The calculation equations, units, ranges, and optimal values of the evaluation indicators are listed in Table 2.

2.3.2. SWAT model

The SWAT model is a semi-distributed, process-based, and time-continuous river basin model (Arnold *et al.* 1998) that can simulate the basin water cycle process (Duan *et al.* 2019), soil erosion (Song *et al.* 2011), and nutrient transportation (Zhang *et al.* 2013; Wang *et al.* 2018). The application of the SWAT model in the YRSR has been recognized (Zhenchun *et al.* 2013; Liu *et al.* 2018; Mengyaun *et al.* 2019). In SWAT, the basin in question is divided into various sub-basins according to the drainage area threshold and then further subdivided into hydrologic response units (HRUs), composed of land portions with the same land use, soil, and slope characteristics. Previous studies have proven that dividing the YRSR into 25 (Liu *et al.* 2018), 29 (Zhenchun *et al.* 2013), and 97 (Mengyaun *et al.* 2019) sub-basins would yield reliable simulation results. Therefore, the YRSR was divided into 25 sub-basins and 1726 HRUs. The HRUs of water balance components, such as precipitation, evapotranspiration, water yield, and surface, lateral, and groundwater flow, were calculated (Neitsch *et al.* 2011). The water balance equation is as follows:

$$SW_{ti} = SW_{oi} + \sum_{i}^{t} (P_i - Qsurf_i - E_i - Wseep_i - Qgw_i) \quad (1)$$

where SW_{ti} is the final soil water content (mm), SW_{oi} is the initial soil water content at time i (mm); t is the time (days); P_i is the amount of precipitation at time i (mm); $Qsurf_i$ is the surface runoff amount at time i (mm); E_i is the amount of evapotranspiration at time i (mm); $Wseep_i$ is the amount of water that enters the vadose zone from the soil profile at time i (mm), and Qgw_i is the return flow amount on day i (mm).

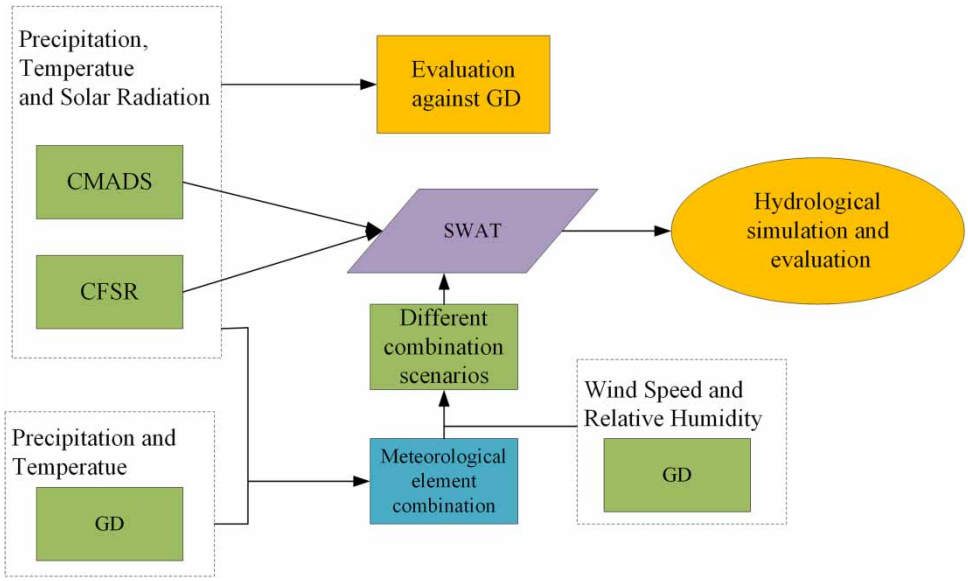

Figure 2 | Flow chart of analytical process.

The time scales of runoff data (2008–2012), CMADS (2008–2016), and CFSR (1976–2014) were comprehensively considered. We selected the simulation period from 2008 to 2012, with a one-year (2008) warm-up period, two-year (2009–2010) calibration period, and two-year (2011–2012) validation period.

2.3.3. Virtual weather station

The numbers of weather station of CMADS, and CFSR located in the YRSR are 198 and 122, respectively. The method for representing weather data in the SWAT model is simplistic, as it only uses data from one weather station that is nearest to the centroid of the sub-basin (Galván *et al.* 2014). It is impractical to divide the watershed into 198 sub-watersheds and correspond thereto on a one-by-one basis. This leads to an inaccurate representation of sub-basin weather input data (Tuo *et al.* 2016). Therefore, virtual weather stations were constructed for each sub-basin that adopted the mean meteorological element of the site within each sub-basin (Ruan *et al.* 2017). The specific methods are as follows:

- Based on the ArcGIS platform, reanalysis station weather data falling in each sub-basin were extracted;
- The arithmetic average method was used to calculate the areal weather data of each sub-basin, giving weather data pertaining to each virtual weather station;
- The centroid of each sub-basin is the location of the virtual weather station (Figure 1).

2.3.4. Meteorological elements combination scenarios

In the present study, 20 scenarios of cross-combined precipitation (GD, CMADS, and CFSR), temperature (GD, CMADS, and CFSR), and solar radiation (CMADS and CFSR) were created, as shown in Table 3. For comparison purposes, the relative humidity and wind speed data for each scenario were derived from GD. Scenarios S1 to S18 were designed to study the performance of meteorological element combination-driven SWAT modeling. The S19 and S20 scenarios were directly driven by the SWAT model using the complete CMADS and CFSR datasets, respectively. Yan *et al.* (2019) reported that the solar radiation data of CFSR were closer to the measured data than those of CMADS; the S6 (GD), S19 (CMADS), and S20 (CFSR) scenarios were used to study the effect of three meteorological datasets on the SWAT output. The detailed combination method is shown in Figure 2.

2.3.5. Parameter calibration and model evaluation

Calibration and uncertainty analysis of the simulation results from the model were performed using Sequential Uncertainty Fitting version 2 (SUFI2) in the SWAT calibration and uncertainty program (SWAT-CUP) (Abbaspour 2015). According to previous studies on hydrological modeling in alpine basins (Zhenchun *et al.* 2013; Bhatta *et al.* 2019; Mengyaun *et al.* 2019; Shuai *et al.* 2019), 27 initial parameters were selected. A total of 18 parameters with high sensitivity were then selected by the Latin hypercube and one-factor-at-a-time sampling (LH-OAT) method for calibration, as shown in Table 1. We selected the daily runoff data of the Tangnaihai streamflow station to calibration and validation of the SWAT model in the runoff simulation. According to Abbaspour (2015), the model was calibrated using three iterations with 400 simulations (a total of 1200 simulations during calibration) using the Nash-Sutcliffe Efficiency (NSE) (Nash & Sutcliffe 1970) and PBIAS as the objective function. The parameter range was modified (narrowed down) after each iteration, according to both new parameters suggested by SWAT-CUP (Tuo *et al.* 2016) and their reasonable physical ranges. More detailed steps of the calibration procedures can be found in Abbaspour (2015). The calculation equations, units, ranges, and optimal values of the objective function are listed in Table 2. The criteria proposed by Moriasi *et al.* (2015) was adopted to classify model performance into the respective categories, 'very good' (NSE$>$0.80; PBIAS$<\pm$5%), 'good' (0.70$<$NSE$\leq$0.80; $\pm$5%$\leq$PBIAS$<\pm$10%), 'satisfactory' (0.50$<$NSE$\leq$0.70; $\pm$10%$\leq$PBIAS$<\pm$15%), and 'unsatisfactory' (NSE$\leq$0.50; PBIAS$\geq\pm$15%).

3. RESULTS AND DISCUSSION

3.1. Evaluation of re-analysis dataset

According to Figure 3, the precipitation and maximum and minimum temperatures of CMADS are clearly underestimated on a monthly scale, while the precipitation of CFSR is significantly overestimated, and the maximum and minimum temperatures of CFSR are underestimated. On the annual scale, compared with GD, the deviation of average annual precipitation and maximum and minimum temperatures in CMADS is 157.02 mm, 3.35 °C, and 2.38 °C, respectively, and that in CFSR is 226.5 mm, 6.03 °C and 0.92 °C, respectively. On the monthly scale, except in March, the solar radiation data of CMADS

Table 1 | Model calibration parameters and initial bound

Parameters	Description	Bound
v_SURLAG.bsn	Surface runoff lag time	[4,10]
r_CN2.mgt	SCS runoff curve value	[30,100]
r_OV_N.hru	Manning's 'n' value for overland flow	[2,10]
v_SMFMX.bsn	Maximum melt rate for snow during the year (occurs on summer solstice)	[2,7]
v_SNO50COV.bsn	Snow water equivalent corresponding to 50% snow cover	[0.1,0.7]
v_TIMP.bsn	Snowpack temperature lag factor	[0.4,1]
v_SMFMN.bsn	Minimum melt rate for snow during the year (occurs on winter solstice)	[0.1,5]
r_CH_S2.rte	Average slope of main channel	[−0.1,0.2]
v_CH_N1.sub	Manning's 'n' value for the tributary channels	[0,0.8]
r_CH_L1.sub	Longest tributary channel length in sub-basin	[−0.1,0.1]
v_REVAPMN.gw	Threshold depth of water in the shallow aquifer for 'revap' to occur (mm)	[120,420]
v_ALPHA_BF.gw	Baseflow alpha factor (days)	[0.1,1]
v_ESCO.hru	Soil evaporation compensation factor	[0,1]
v_RCHRG_DP.gw	Deep aquifer percolation fraction	[0,0.6]
r_SLSUBBSN.hru	Average slope length	[−0.2,0.1]
v_GW_DELAY.gw	Hysteresis coefficient of groundwater	[0,500]
v_GW_REVAP.gw	Groundwater 'revap' coefficient	[0,1]
v_GWQMN.gw	Runoff coefficient of shallow groundwater	[0,500]

Note: v=Replace, r=Relative change.

Table 2 | Evaluation indicators of reanalysis meteorological dataset and SWAT model

Category	Diagnostic statistic	Equation	Range of index	Perfect of value	Unit
Meteorological element evaluation	RMSE	$RMSE = \sqrt{\frac{\sum_{i=1}^{n}(P_i - O_i)^2}{n}}$	0–+∞	0	mm
	PBIAS	$PBIAS = \frac{\sum_{i=1}^{n}(R_i - O_i)}{\sum_{i=1}^{n} O_i} \times 100\%$	−∞–+∞	0	%
	CC	$CC = \frac{\sum_{i=1}^{n}(O_i - \bar{O})(R_i - \bar{R})}{\sqrt{\sum_{i=1}^{n}(O_i - \bar{O})^2}\sqrt{\sum_{i=1}^{n}(R_i - \bar{R})^2}}$	−1–1	1	–
Model evaluation	NSE	$NSE = 1 - \frac{\sum_{i=1}^{n}(Q_i^o - Q_i^s)}{\sum_{i=1}^{n}(Q_i^o - \overline{Q_o})}$	−∞–1	1	–
	PBIAS	$PBIAS = \frac{\sum_{i=1}^{n}(Q_i^o - Q_i^s)}{\sum_{i=1}^{n} Q_i^o} \times 100\%$	−∞–1	0	%

Note: n means the number of samples; R_i means the value of a meteorological element in the reanalysis dataset on day i; Q_i means the value of a meteorological element in the GD on day i; $\bar{R}$ means the average value of a meteorological element of the reanalysis dataset; $\bar{O}$ means the average value of a meteorological element of the GD; Q_i^o and Q_i^s respectively represents the observed and simulation streamflow on day i; $\overline{Q_o}$ and $\overline{Q_s}$ respectively represents the average value of observed and simulation streamflow.

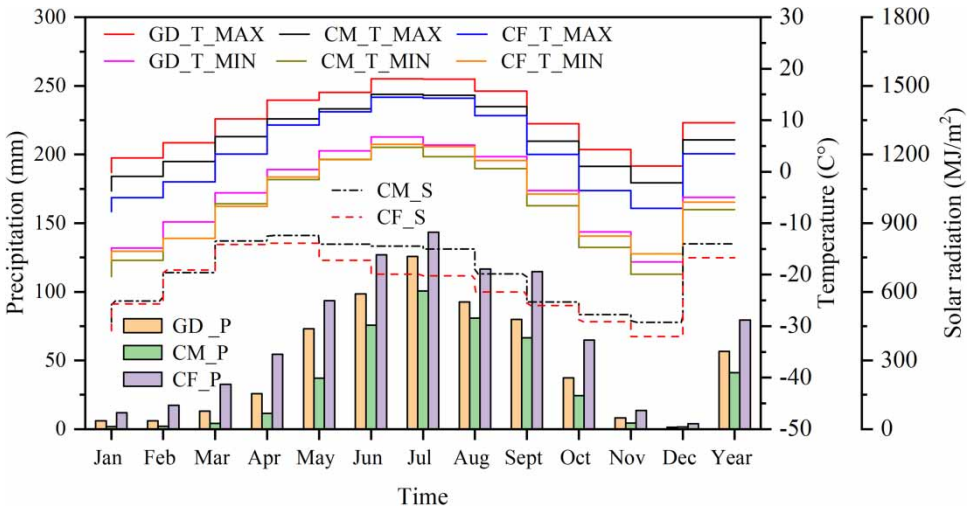

Figure 3 | The average values of meteorological elements (precipitation, maximum temperature, minimum temperature, and solar radiation) from multi-stations at various time scales (monthly and yearly) for different meteorological datasets (GD, CMADS and CFSR) during the period January 1, 2008 to December 31, 2012 in the YRSR. *Note*. GD_P means gauge precipitation, CM_T_MAX means CMADS maximum temperature, CF_T_MIN means CFSR minimum temperature, CM_S means CMADS solar radiation, and so forth. For better display, the annual precipitation and solar radiation data are divided by 10.

were higher than those of CFSR, and the average annual solar radiation deviation of CFSR was 598.8 MJ/m^2 compared with CMADS.

To further reflect the difference between the precipitation and temperature of the re-analysis datasets and the GD, the PBIAS, CC, and RMSE of the re-analysis datasets and the GD were counted at monthly and yearly timescales. Based on Figure 4(a1) and (a2), the deviation of precipitation between re-analysis datasets and GD was generally lower during the wet season (May–November) than during the dry season. In contrast, the deviation degree of CFSR was greater than that of CMADS. The RMSE of re-analysis datasets during the wet season was greater than those from the dry season. The correlation between CFSR and GD was significantly larger than that between CMADS and GD at the monthly scale, and the CMADS was negatively correlated with observed data in most months. As seen in Figure 4(b1) and (b2), the maximum temperature of CMADS and CFSR was underestimated except in January, and the PBIAS value in January was considerably higher than in other months. The RMSE values of the maximum temperature ranged from 2.99 to 3.62 °C for CMDAS and from 3.58 to 8.36 °C for CFSR at the monthly scale. The minimum temperatures of CMADS and CFSR were underestimated during the rainy season (May–September), especially in May (Figure 4(c1) and (c2)). On the monthly scale, the CC values of the two datasets varied greatly from month to month in terms of maximum and minimum temperatures, and the CC values in the rainy season were larger than those in other months. On the annual scale, the statistical metrics demonstrated that the maximum temperature from CMADS was of higher quality than that from CFSR, while the minimum temperature from CFSR was better than that from CMADS. Overall, the temperature data of the CFSR and CMADS were weakly correlated with the gauge data. The reason for this phenomenon may be due to the fact that most weather stations are located at low altitudes, which cannot effectively reflect the temperature characteristics in YRSR. Li *et al.* (2003) reported that elevation is a key factor affecting the temperature interpolation algorithm in the Qinghai-Tibet Plateau. Regarding the above analysis, the quality of precipitation and temperature of the CMADS and CFSR in the rainy season was higher than that in other months.

3.2. Effect of different meteorological elements as the input

3.2.1. Effect of different precipitation as input

According to Figure 5(a)–(c), the precipitation element has a significant impact on SWAT modeling since the average NSE values of the scenarios inputted with GD precipitation (S1–S6) in the calibration/validation period were 0.83/0.80, followed by CFSR (S13–S18) at 0.65/0.54, the worst being CMADS (S7–S12) at 0.18/0.45. The runoff simulated using CMADS and CFSR precipitation was obviously underestimated (average PBIAS=48.51%) and overestimated (average PBIAS=-15.09%), respectively. Additionally, in the rainy season, the runoff simulated by CFSR precipitation has a phenomenon of fast rise

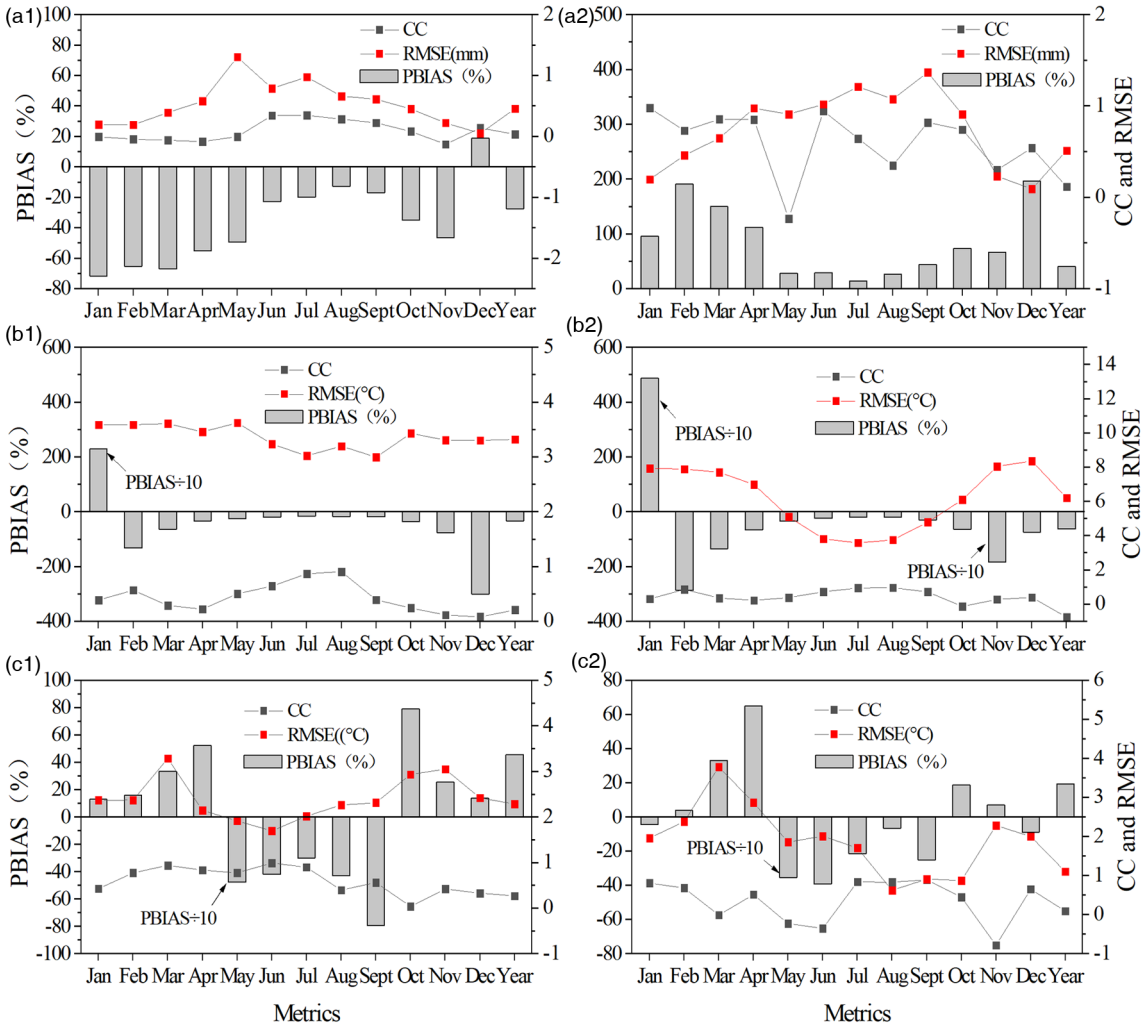

Figure 4 | The metrics of multi-station average: (a) precipitation, (b) maximum temperature, and (c) minimum temperature comparing the gauge data with the (1) CMADS and (2) CFSR at various time scales in the YRSR.

and steep fall (Figure 5(c)–(h)). This may be because CFSR often overestimated the extreme precipitation (Zhu *et al.* 2016a), so do extreme streamflow simulations forced with it.

The S6, S12, and S18 scenarios were selected for comparison and to analyze the influence of three different precipitation on the simulation results. Based on Figure 6(d)–(f), the best performance was with a model with GD precipitation, followed by CFSR and CMADS. The precipitation input into the SWAT model by GD, CMADS, and CFSR was 519.24, 412.51, and 768.07 mm (Figure 6(i)), respectively. Among them, the GD precipitation was the closest to the actual precipitation in YRSR (Hu *et al.* 2011), explaining why the input scenarios with GD precipitation show better simulation results than others (Table 3). The S6 scenario, using GD precipitation (albeit with sparse coverage), yielded good performance with NSE of 0.79–0.80 and PBIAS of 5.1–8.6%. This may be due to fewer human activities in the YRSR, so the sparse observation stations in the YRSR can reflect changes in runoff (Mingxing *et al.* 2018). Using CMADS precipitation (S12) resulted in unsatisfactory simulated daily streamflow with substantial underestimation in both calibration (PBIAS=50.6%) and validation (PBIAS=46.4%) periods. This was mainly due to the underestimation in precipitation and temperature by CMADS (Figures 3 and 4), resulting in low SNOW and PERC values calculated by the model (Figure 6(i)). The scenarios (S18) inputted with CFSR precipitation yielded good performance for the calibration period, but the performance was slightly worse for the validation period with satisfactory performance. This is a good phenomenon because the CFSR product tended to overestimate precipitation and resulted in unsatisfactory runoff simulation using hydrological models (Meng *et al.* 2016; Zhu *et al.* 2016b; Hu *et al.* 2017; Poméon *et al.* 2017; Chen *et al.* 2018; Tan *et al.* 2018a).

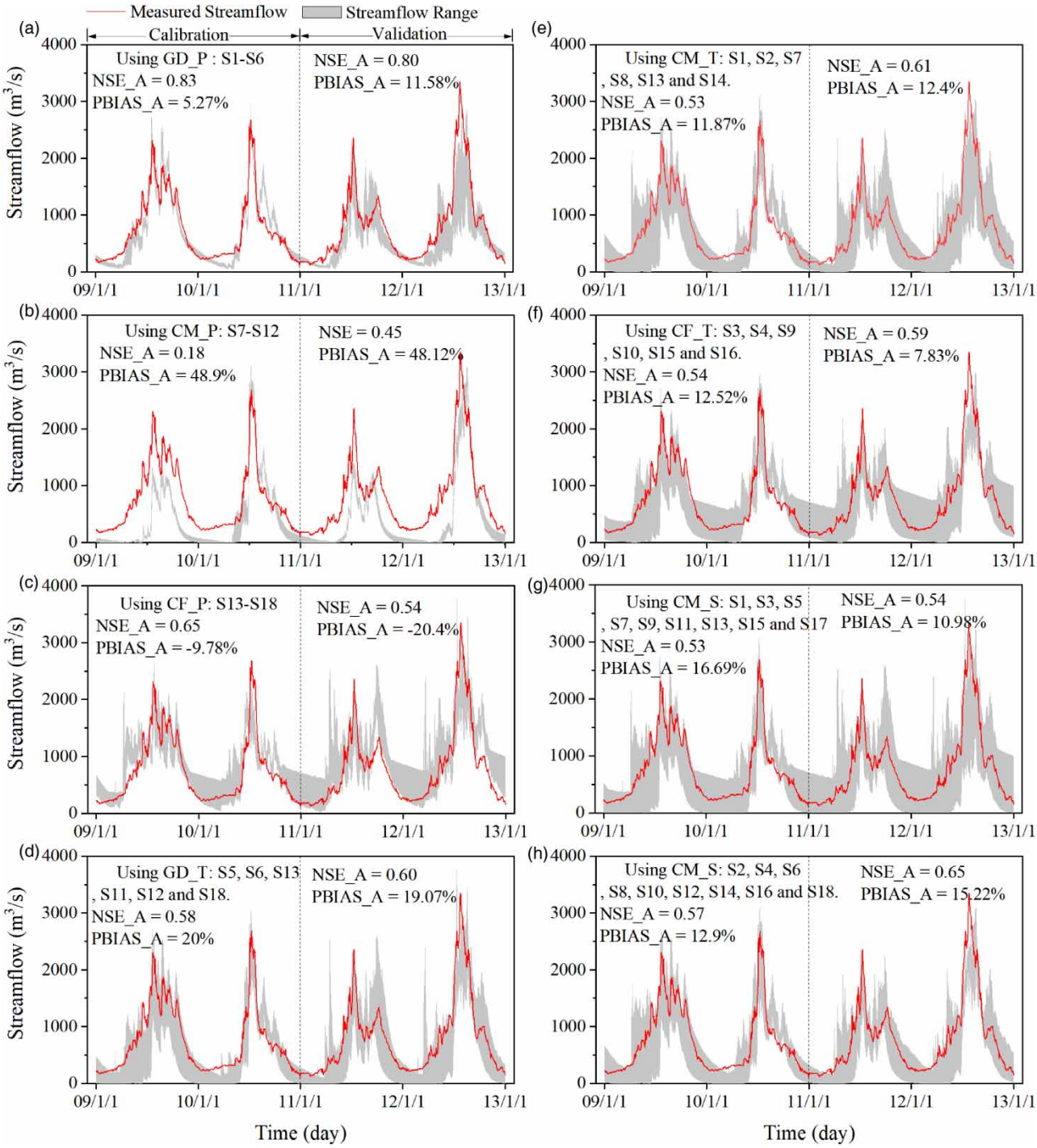

Figure 5 | Daily streamflow simulation under 18 meteorological element combination scenarios. *Note*. NSE_A means the average values of NSE, PBIAS_A means the average values of PBIAS.

3.2.2. Effect of different temperatures as input

By combining the results of Figure 5, temperature had a smaller influence on the model simulation results than precipitation. The average NSE values of the scenarios inputted with the GD, CMADS, and CFSR temperatures for the calibration/validation periods were 0.58/0.60, 0.53/0.61, and 0.54/0.59, respectively (Figure 5(d)–(f)). Based on Moriasi *et al.* (2015), the scenarios using CFSR temperature as input perform best, followed by those using CMADS and GD.

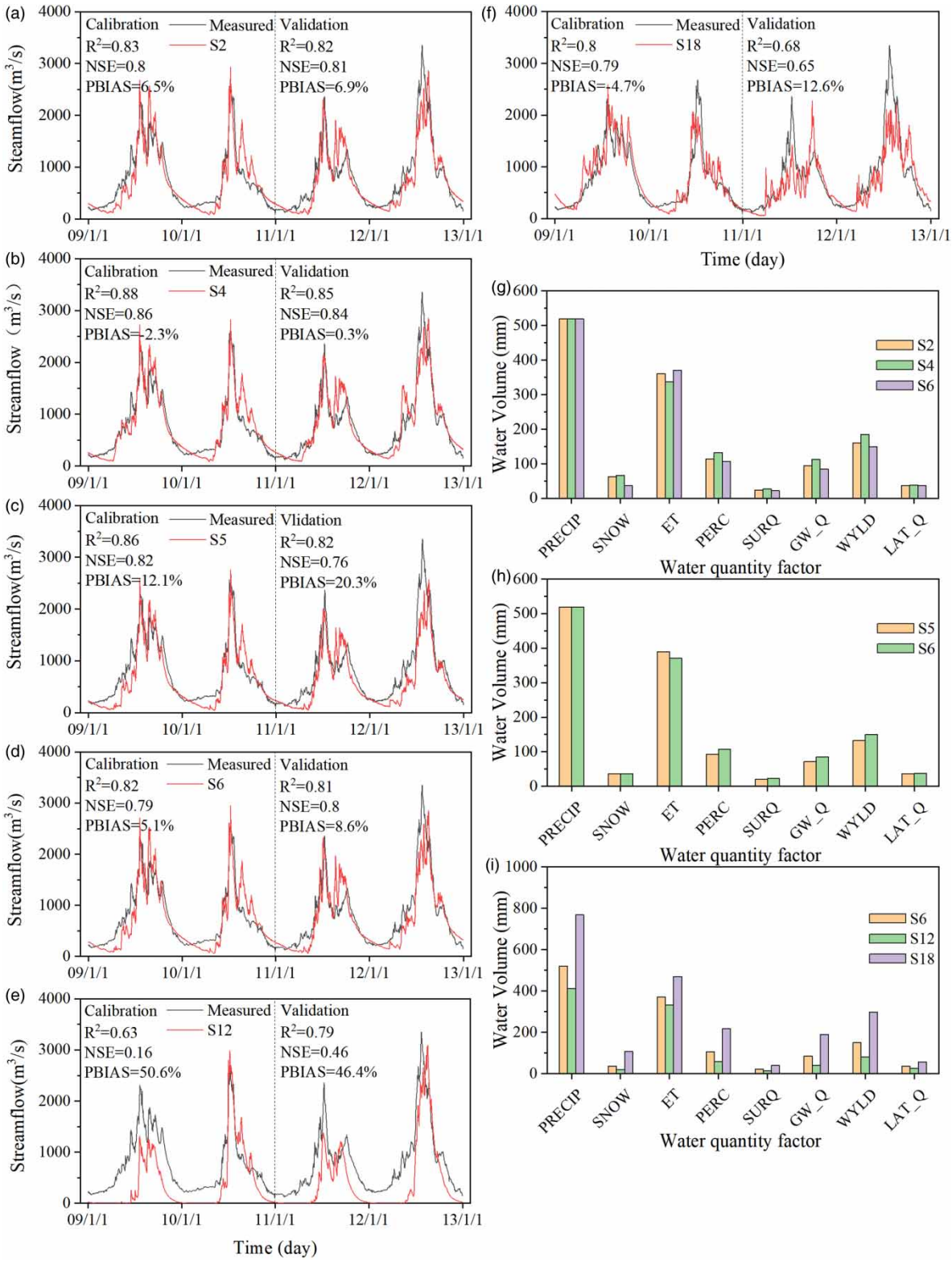

Figure 6 | Daily streamflow simulation under typical meteorological element combination scenarios, and output analysis of water balance for models. *Note*: PREC means the total precipitation on basin (mm); SNOW means the amount of snow or ice melting (mm); ET means the amount of water removed by evapotranspiration (mm); PERC means the amount of water percolating out of the root zone (mm); SURQ means the surface runoff (mm); GW_Q means the groundwater discharge into reach (mm); WYLD means the net amount of water contributed by the HRU to the reach (mm H_2O); LAT_Q means the lateral flow contribution to reach(mm).

Table 3 | Summary of the combined scenarios of precipitation, temperature, and solar radiation and simulation results of SWAT model driven by each scenario at the daily scales

	Meteorology elements			Calibration			Validation		
Scenario	Precipitation	Temperature	Solar Radiation	NES	PBIAS(%)	Performance	NES	PBIAS(%)	Performance
1	GD_P	CM_T	CM_S	0.81	6.5	★★	0.79	19.6	
2			CF_S	0.8	3.4	★★	0.81	6.9	★★
3		CF_T	CM_S	0.87	6.8	★★	0.8	13.8	★
4			CF_S	0.86	−2.3	★★★	0.84	0.3	★★★
5		GD_T	CM_S	0.82	12.1	★	0.76	20.3	
6			CF_S	0.79	5.1	★★	0.8	8.6	★★
7	CM_P	CM_T	CM_S	0.14	51.9		0.4	51.4	
8			CF_S	0.2	48.5		0.5	45.9	
9		CF_T	CM_S	0.2	45.3		0.43	49.2	
10			CF_S	0.26	42.1		0.54	42	
11		GD_T	CM_S	0.09	55		0.37	53.8	
12			CF_S	0.16	50.6		0.46	46.4	
13	CF_P	CM_T	CM_S	0.62	−13.8	★	0.49	−39.1	
14			CF_S	0.62	−25.3		0.64	−10.3	★
15		CF_T	CM_S	0.41	−15.5		0.28	−42.9	
16			CF_S	0.64	−1.3	★	0.65	−15.4	
17		GD_T	CM_S	0.8	1.9	★★	0.55	−27.3	
18			CF_S	0.79	−4.7	★★	0.65	12.6	★
19	CMADS	0.13	53		0.39	52.3			
20	CFSR	0.41	−18		0.27	−46.8			

Note: ★★★ very good performance, ★★ good performance, ★ satisfactory performance.

We selected S2, S4, and S6 for comparison and to analyze the influence of three different temperature on the simulation results. According to Figure 6(a)–(c), the S4 scenarios that use CFSR temperature as input showed the best performance and yielded outstanding performance over the entire period. However, using GD (S6) and CMADS (S2) resulted in a good performance, and in contrast, the S6 scenario was superior to S2. This was mainly because the temperatures of CMADS and CFSR were underestimated (Figures 3 and 4), resulting in the low evapotranspiration and high streamflow calculated by the SWAT model (Figure 6(g)). According to SWAT model theory, temperature mainly affects the calculation of evapotranspiration and snowmelt runoff (Neitsch *et al.* 2002). However, the snowmelt module of the SWAT model was not ideal in the YRSR, as it could not reflect the changes in temperature (Figure 6(g)). The SNOW values of the scenarios inputted as GD, CMADS, and CFSR temperature were 36.63, 62.82, and 66.67 mm, respectively. This may be because SWAT was originally developed to evaluate water resources in large agricultural basins, and was not designed to model heterogeneous mountain basins typical of the alpine basins (Fontaine *et al.* 2002). Zhenchun *et al.* (2013) have greatly improved the simulation accuracy by adjusting the snowmelt module of the SWAT model. The WYLD values of the scenarios inputted as GD, CMADS, and CFSR temperature were 149.83, 160.64, and 184.44 mm, respectively (Figure 6(g)). This shows the favorable accuracy of CMADS and CFSR temperature for hydrological modeling in the YRSR, which is good news for the local hydrometeorological department as the quality of the observed temperature is often worse than that of precipitation (Duan *et al.* 2019).

3.2.3. Effect of different solar radiation as input

Scenarios S5 and S6 were selected to determine the effects of different solar radiation on SWAT outputs. As shown in Figure 6(c) and (d), we found that solar radiation has a slight influence on the model simulation results in terms of NSE. The average NSE values of the scenarios inputted with CMADS and CFSR solar radiation data for the calibration/validation periods were 0.53/0.54 and 0.57/0.65, respectively (Figure 5(g) and (h)). However, the PBIAS values of S5 and S6 were quite

different. The S6 scenario resulted in decent performance with PBIAS of less than 10%, while the S5 scenario yielded satisfactory performance for the calibration period (PBIAS=12.1%) and unsatisfactory performance for the validation periods (PBIAS=20.1%). This is primarily because the solar radiation data of CMADS were greater than those of CFSR (Figure 3), resulting in large evapotranspiration and small runoff for S5, as calculated by the SWAT model (Figure 6(h)). Solar radiation mainly affects the evapotranspiration calculation of the hydrological model, thus changing the process of water balance (Neitsch *et al.* 2002). The SWAT model has three methods to calculate evapotranspiration, namely, Penman-Monteith, Priestley-Taylor, and Hargreaves. The Penman-Monteith method was adopted in this paper. Tian *et al.* (2018) found that the evapotranspiration calculated by the Penman-Monteith method based on CMADS solar radiation data in western China is overestimated by 15–30%. This conclusion was verified through the unselected scenarios (Table 3). Regarding the above analysis, the solar radiation data from CFSR and CMADS in the YRSR could drive the hydrological model, and the CFSR data are more suitable for hydrological simulation in YRSR than that from CMADS.

3.2.4. Effect of different meteorological datasets as input

Apparently, using GD (even with sparse coverage) as input to drive SWAT resulted in the best daily streamflow simulation in the YRSR (Figure 6(d)), followed by CFSR (Figure 7(b1)) and CMADS (Figure 7(a1)). The findings of this study differ from those of previous studies, which reported that the SWAT models driven by CMADS have a better performance in the research basin (Gao *et al.* 2018b; Zhou *et al.* 2019). However, the performance of CMADS and CFSR was poor, with clear underestimation (PBIAS$\geq$52.3%) for CMADS and overestimation (PBIAS$\leq-$18%) for CFSR, especially in the dry season. Similarly, Yu & Mu (2015) reported that the runoff simulated by the SWAT model driven by CFSR in alpine regions was overestimated, and Wang *et al.* (2020) found that the runoff simulation results driven by CMADS were severely underestimated. This is mainly because CMADS and CFSR precipitation is underestimated and overestimated, respectively (Figures 3 and 4), leading to the precipitation of the input SWAT model being small for CMADS and large for CFSR (Figure 6(i)). Additionally, CMADS (Meng *et al.* 2018) and CFSR (Saha *et al.* 2014; Radcliffe & Mukundan 2017) are generated by interpolation methods based on observation and satellite remote sensing data, and the interpolation accuracy is greatly affected by the density of the regional stations and topography (Dodson & Marks 1997). The elevation of the meteorological stations for the YRSR and surrounding area was lower than the average elevation, and the observatory density was low and uneven (Figure 1(c)).

Interestingly, after careful comparison, we found that the simulation results of S19 and S20 could be effectively improved by replacing the meteorological elements (Figure 7(a2), (a3), (b2) and (b3)), especially for CFSR. In the S18 scenario, the model using CFSR precipitation, GD temperature, and CFSR solar radiation as input had good performance for the calibration period and satisfactory performance for the validation period (Figure 7(b2)). Similarly, the S17 model using CFSR precipitation, GD temperature, and CMADS solar radiation as input yielded good performance for the calibration periods (Figure 7(b3)). Based on Figure 7(b4), it is clear that evapotranspiration in S17 and S18 is greater than that in S20, and SNOW, PERC and GW_Q in S20 are greater than those in S17 and S18; therefore, S20 translated more precipitation into runoff than S17 and S18. This was due to the underestimation of CFSR temperature (Figures 3 and 4), and the CMADS solar radiation, which was greater than that of CFSR (Figure 3), resulting in the large evapotranspiration and low streamflow calculated by the SWAT model. These results indicate that the improvement of hydrological model accuracy is not only in seeking precipitation products with high spatial-temporal accuracy (Tan *et al.* 2018b; Yuan *et al.* 2018; Guo *et al.* 2019) or correcting precipitation data (Hu *et al.* 2017; Deng *et al.* 2019; Wang *et al.* 2020) but also in improving the model accuracy through a combination of meteorological inputs.

3.3. Discussion with existing studies in the same area

A literature search showed that, to date, several studies had been carried out to evaluate the performance of different weather or precipitation datasets in driving hydrological models (particularly the SWAT model) to simulate runoff in the YRSR, as shown in Table 4. We discussed our results with the most relevant previous studies that considered the same weather datasets (GD, CMADS, and CFSR) as in our study.

Liu *et al.* (2018) evaluated the performance of different weather datasets, including GD, CMADS, and CFSR, in driving the SWAT model in runoff simulations in the same basin and reported that SWAT driven by CMADS and CFSR was better than that driven by GD. The evaluation statistics showed that the NSE values of CMADS at the daily scale were 0.63 and 0.59 for the calibration and validation periods, respectively, while those of GD were -0.72 and -0.91. This is contrary to our findings where GD-driven SWAT produced the best output, with NSE of 0.79–0.80 in YRSR, followed by CFSR with NSE of

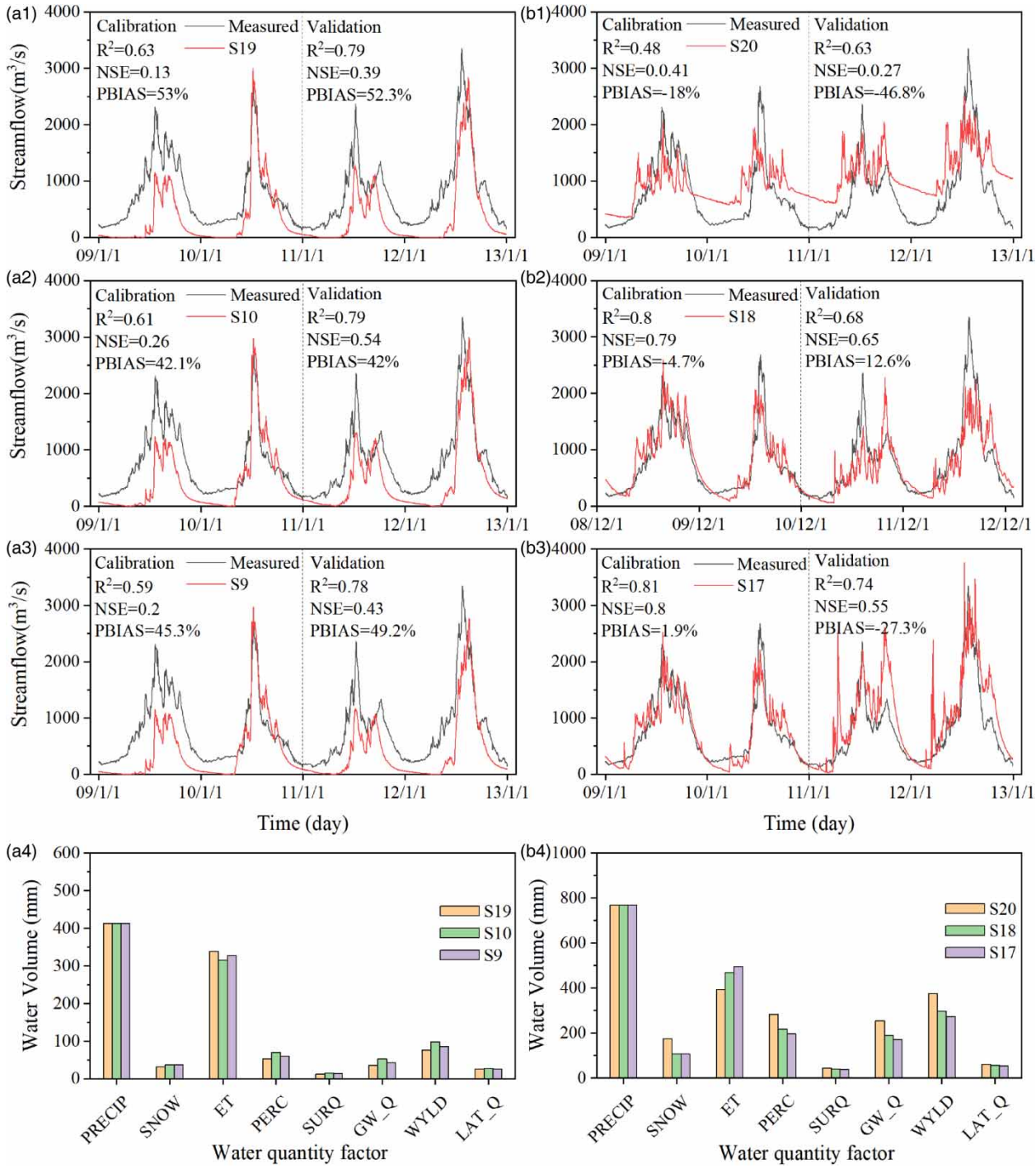

Figure 7 | Daily streamflow simulation under typical CMADS and CFSR precipitation scenarios, and output analysis of water balance for models.

0.27–0.41, and CMADS with an NSE of 0.12–0.39 (Table 3). This could be mainly due to three reasons. First, and most importantly, Liu *et al.* (2018) used an old version of the CMADS (1.0) dataset, whereas our study used the CMADS version 1.1 dataset. Although existing studies have shown that the new version performs better than the old version and has reasonably good agreement with measured runoff, most were concentrated in basins in northern China, such as the Heihe River Basin (Meng *et al.* 2019), Manas River Basin (Meng *et al.* 2017), Jing and Bortala River Basin (Li *et al.* 2019), Northeast basin

Table 4 | Simulation results of hydrological model driven by different meteorological datasets or precipitation products in the YRSR

Study	Model	Evalution period	Temporal scales	Data	NSE	PBIAS(%)	R^2
Yuan *et al.* (2018)	Xinanjiang	2014.4 to 2016.12	Daily	GD	0.23 to 0.89	−5.1 to 29.7	/
				IMERG	0.59 to 0.84	1.8 to 14.5	/
				TRMM_3B42V7	0.23 to 0.80	6.6 to 21.6	/
Liu *et al.* (2018)	SWAT	2009 to 2013	Daily	GD	−0.91 to −0.72	/	0.43 to 0.46
				CMADS	0.59 to 0.63	/	0.71 to 0.83
				CFSR	0.42 to 0.47	/	0.58 to 0.65
Zhenchun *et al.* (2013)	SWAT	1960 to 1990	Monthly	GD	0.51 to 0.91	−30 to −8	/
Wei *et al.* (2016)	VIC	1991 to 2010	Monthly	GD	0.83 to 0.85	/	/
Mengyaun *et al.* (2019)	SWAT	1970 to 2012	Monthly	GD	0.80 to 0.81	/	/
Shuai *et al.* (2019)	SWAT	1977 to 1986	Monthly	GD	0.75 to 0.81	/	/
This study	SWAT	2008 to 2012	Daily	GD	0.79 to 0.80	5.1 to 8.6	/
				CMADS	0.13 to 0.39	52.3 to 53	/
				CFSR	0.27 to 0.41	−18 to −46.8	/

(Zhang *et al.* 2020) and Lijiang River Basin (Cao *et al.* 2018). In the Jinsha River Basin, Guo *et al.* (2019) reported that simulated runoff driven by CMADS only resulted in satisfactory performance with an NSE of 0.5, which is not as good as in previous studies (Li *et al.* 2019; Meng *et al.* 2019; Zhang *et al.* 2020). Notably, in the Xihe River Basin, located in the Qinling Mountains, Wang *et al.* (2020) found that the monthly streamflow simulation by SWAT driven by CMADS precipitation (1.1) had poor performance with an NSE of –0.43 and PBIAS of 95.22%. These results indicate that the regional heterogeneity of CMADS is significant and that it is necessary to evaluate the accuracy of CMADS before use. Second, Liu *et al.* (2018) used only 11 meteorological stations in the study area, whereas our study used 14. Previous studies have shown that the accuracy of meteorological data directly affects the simulation results of hydrological models (Wagner *et al.* 2012; Tuo *et al.* 2016; Laiti *et al.* 2018). Previous studies have proven that hydrological models driven by GD yielded ideal simulation results in the YRSR (Table 4). Third, in addition to the difference in weather dataset input for the SWAT model, the calibration strategies used by Liu *et al.* (2018) might not be able to find the optimal values for each dataset, although they did not explicitly detail the calibration procedures, but simply mentioned that 12 sensitive parameters were selected for calibration. Our study used more parameters (Table 1) and more objective calibration with the same starting parameter boundary in a sufficient number of iterations, which increases the possibility of finding optimal parameter values for each model.

4. CONCLUSIONS

(1) Compared with GD, CFSR precipitation and temperature are overestimated and underestimated, respectively, while those of CMADS are all underestimated.
(2) Among the three meteorological elements of precipitation, temperature, and solar radiation, precipitation had the greatest impact on the outcome of the SWAT runoff simulation. Using GD precipitation from sparse stations consistently yielded better performance than precipitation from CMADS and CFSR in the YRSR.
(3) Compared with precipitation elements, temperature and solar radiation elements slightly influence SWAT runoff simulation. Among the temperature data of the three meteorological datasets, CFSR temperature was the best in runoff simulation, followed by CMADS and GD. In contrast, CFSR solar radiation is more suitable for hydrological simulation in the YRSR than that of CMADS.

(4) Although SWAT modeling driven by CMADS and CFSR performed poorly with clear underestimation (PBIAS≥52.3%) for CMADS and overestimation (PBIAS≤−18%) for CFSR, the temperature and solar radiation of CMADS and CFSR can be alternative data sources for streamflow simulation in the YRSR.
(5) Comparing all scenarios comprehensively, the SWAT model driven by the combination of GD precipitation, CFSR temperature, and CFSR solar radiation performed best, with an NSE of 0.84–0.86 and PBIAS of 2.3–0.3%.
(6) Taken together, the SWAT model driven by combined datasets of different meteorological elements is effective. The method of driving hydrological models by combining multi-source meteorological elements is of great significance not only for hydrological-runoff simulation due to the lack of observation basins but also for observing intensive basins. This is because it is easier to optimize and correct meteorological products for multi-source satellite-based and reanalysis-based products on a large amount of measured data.

According to Figures 5 and 6, the snowmelt module of the SWAT model was not ideal in the YRSR model, as it could not reflect the changes in temperature (Figure 6(g)) and solar radiation (Figure 6(h)), and spring runoff was underestimated (Figure 5(a)). Additionally, the scarcity of meteorological data in the alpine basin is common, and it is difficult to improve in a short time. Exploring alternative meteorological datasets that are more feasible, such as satellite meteorological data with high spatial-temporal resolution, is a good way to improve hydrological model simulations. Therefore, we can optimize hydrological model research for alpine watersheds from the aspects mentioned above.

DECLARATION OF INTEREST STATEMENT

All authors declare that there is no financial or personal interest or belief that could affect our objectivity. We declare that we have no conflict of interest.

ACKNOWLEDGEMENTS

This work was supported by National Key Research and Development Program of China (grant numbers: 2016YFA0601703 and 2016YFC0401005) and Nation Nature Science Foundation of China (grant numbers: 91847301, 92047203). Acknowledgement for the data support form 'National Earth System Science Data Center, National Science & Technology Infrastructure of Chia. (http://www.geodata.cn)'

DATA AVAILABILITY STATEMENT

All relevant data are available from an online repository or repositories.

REFERENCES

Abbaspour, K. 2015 SWAT-Calibration and uncertainty programs (CUP). *Neprashtechnology. Ca.* https://doi.org/10.1007/s00402-009-1032-4.

Arnold, J. G., Srinivasan, R., Muttiah, R. S. & Williams, J. R. 1998 Large area hydrologic modeling and assessment part I: model development. *J. Am. Water Resour. Assoc.* https://doi.org/10.1111/j.1752-1688.1998.tb05961.x.

Auerbach, D. A., Easton, Z. M., Walter, M. T., Flecker, A. S. & Fuka, D. R. 2016 Evaluating weather observations and the Climate Forecast System Reanalysis as inputs for hydrologic modelling in the tropics. *Hydrol. Process.* https://doi.org/10.1002/hyp.10860.

Awange, J. L., Hu, K. X. & Khaki, M. 2019 The newly merged satellite remotely sensed, gauge and reanalysis-based Multi-Source Weighted-Ensemble Precipitation: Evaluation over Australia and Africa (1981–2016). *Sci. Total Environ.* https://doi.org/10.1016/j.scitotenv.2019.03.148.

Bajracharya, S. R., Palash, W., Shrestha, M. S., Khadgi, V. R., Duo, C., Das, P. J. & Dorji, C. 2015 Systematic evaluation of satellite-based rainfall products over the Brahmaputra basin for hydrological applications. *Adv. Meteorol.* https://doi.org/10.1155/2015/398687.

Bhatta, B., Shrestha, S., Shrestha, P. K. & Talchabhadel, R. 2019 Evaluation and application of a SWAT model to assess the climate change impact on the hydrology of the Himalayan River Basin. *Catena*. https://doi.org/10.1016/j.catena.2019.104082.

Cao, Y., Zhang, J., Yang, M., Lei, X., Guo, B., Yang, L., Zeng, Z. & Qu, J. 2018 Application of SWAT model with CMADS data to estimate hydrological elements and parameter uncertainty based on SUFI-2 algorithm in the Lijiang River basin, China. *Water (Switzerland)*. https://doi.org/10.3390/w10060742.

Chen, A., Chen, D. & Azorin-Molina, C. 2018 Assessing reliability of precipitation data over the Mekong River Basin: a comparison of ground-based, satellite, and reanalysis datasets. *Int. J. Climatol.* https://doi.org/10.1002/joc.5670.

Dao, D. M., Lu, J., Chen, X., Kantoush, S. A., Binh, D. V., Phan, P. & Tung, N. X. 2021 Predicting tropical monsoon hydrology using CFSR and CMADS data over the Cau River Basin in Vietnam. *Water* **13**, 1314. https://doi.org/10.3390/w13091314.

De Almeida Bressiani, D., Srinivasan, R., Jones, C. A. & Mendiondo, E. M. 2015 Effects of different spatial and temporal weather data resolutions on the stream flow modeling of a semi-arid basin, Northeast Brazil. *Int. J. Agric. Biol. Eng.* https://doi.org/10.3965/j.ijabe.20150803.970.

Deng, P., Zhang, M., Bing, J., Jia, J. & Zhang, D. 2019 Evaluation of the GSMaP_Gauge products using rain gauge observations and SWAT model in the Upper Hanjiang River Basin. *Atmos. Res.* **219**, 153–165. https://doi.org/10.1016/j.atmosres.2018.12.032.

Dodson, R. & Marks, D. 1997 Daily air temperature interpolated at high spatial resolution over a large mountainous region. *Clim. Res.* https://doi.org/10.3354/cr008001.

Duan, Z., Tuo, Y., Liu, J., Gao, H., Song, X., Zhang, Z., Yang, L. & Mekonnen, D. F. 2019 Hydrological evaluation of open-access precipitation and air temperature datasets using SWAT in a poorly gauged basin in Ethiopia. *J. Hydrol.* **569**, 612–626. https://doi.org/10.1016/j.jhydrol.2018.12.026.

Eini, M. R., Javadi, S., Delavar, M., Monteiro, J. A. F. & Darand, M. 2019 High accuracy of precipitation reanalyses resulted in good river discharge simulations in a semi-arid basin. *Ecol. Eng.* https://doi.org/10.1016/j.ecoleng.2019.03.005.

Famiglietti, J. S., Cazenave, A., Eicker, A., Reager, J. T., Rodell, M. & Velicogna, I. 2015 Satellites provide the big picture. *Science (80-.)*. https://doi.org/10.1126/science.aac9238.

Fontaine, T. A., Cruickshank, T. S., Arnold, J. G. & Hotchkiss, R. H. 2002 Development of a snowfall-snowmelt routine for mountainous terrain for the soil water assessment tool (SWAT). *J. Hydrol.* **262**, 209–223. https://doi.org/10.1016/S0022-1694(02)00029-X.

Fuka, D. R., Walter, M. T., Macalister, C., Degaetano, A. T., Steenhuis, T. S. & Easton, Z. M. 2014 Using the climate forecast system reanalysis as weather input data for watershed models. *Hydrol. Process.* https://doi.org/10.1002/hyp.10073.

Galván, L., Olías, M., Izquierdo, T., Cerón, J. C. & Fernández de Villarán, R. 2014 Rainfall estimation in SWAT: an alternative method to simulate orographic precipitation. *J. Hydrol.* **509**, 257–265. https://doi.org/10.1016/j.jhydrol.2013.11.044.

Gao, C., Liu, L., Wang, Z. & Xu, Y. 2018a Precipitation bias-correction methods for Yellow River basin upstream of Tangnaihai. *Shuili Fadian Xuebao/Journal Hydroelectr. Eng.* **37**, 29–39. https://doi.org/10.11660/slfdxb.20180904 (In Chinese).

Gao, X., Zhu, Q., Yang, Z. & Wang, H. 2018b Evaluation and hydrological application of CMADS against TRMM 3b42v7, PERSIANN-CDR, NCEP-CFSR, and gauge-based datasets in Xiang River basin of China. *Water (Switzerland)*. https://doi.org/10.3390/w10091225.

Guo, D., Wang, H., Zhang, X. & Liu, G. 2019 Evaluation and analysis of grid precipitation fusion products in Jinsha river basin based on China meteorological assimilation datasets for the SWAT model. *Water (Switzerland)*. https://doi.org/10.3390/w11020253.

Hu, Y., Maskey, S., Uhlenbrook, S. & Zhao, H. 2011 Streamflow trends and climate linkages in the source region of the Yellow River, China. *Hydrol. Process.* https://doi.org/10.1002/hyp.8069.

Hu, S., Qiu, H., Yang, D., Cao, M., Song, J., Wu, J., Huang, C. & Gao, Y. 2017 Evaluation of the applicability of climate forecast system reanalysis weather data for hydrologic simulation: a case study in the Bahe River Basin of the Qinling Mountains, China. *J. Geogr. Sci.* https://doi.org/10.1007/s11442-017-1392-6.

Immerzeel, W. W., Van Beek, L. P. H. & Bierkens, M. F. P. 2010 Climate change will affect the asian water towers. *Science (80-.)*. https://doi.org/10.1126/science.1183188.

Laiti, L., Mallucci, S., Piccolroaz, S., Bellin, A., Zardi, D., Fiori, A., Nikulin, G. & Majone, B. 2018 Testing the hydrological coherence of high-Resolution gridded precipitation and temperature data sets. *Water Resour. Res.* https://doi.org/10.1002/2017WR021633.

Li, X., Chen, G. & Lu, L. 2003 Comparison study of spatial interpolation methods of air temperature over Qinghai-Xizang Plateau. *Plateau Meteorol.* **22**, 565–573. https://doi.org/1000-0534(2003)06-0565-09.

Li, Y., Wang, Y., Zheng, J. & Yang, M. 2019 Investigating spatial and temporal variation of hydrological processes in western China driven by CMADS. *Water (Switzerland)* **11**. https://doi.org/10.3390/w11030435.

Liu, X. & Chang, X. 2005 A summary of study on runoff variations in source region of the Yellow River. *Yellow River* **27**, 6–12. https://doi.org/1000-1379(2005)02-0006-03.

Liu, J., Shanguan, D., Liu, S. & Ding, Y. 2018 Evaluation and hydrological simulation of CMADS and CFSR reanalysis datasets in the Qinghai-Tibet Plateau. *Water (Switzerland)*. https://doi.org/10.3390/w10040513.

Meng, X., Shi, C., Liu, S., Wang, H., Lei, X., Liu, Z., Ji, X., Cai, S. & Zhao, Q. 2016 CMADS datasets and Its application in watershed hydrological simulation: a case study of the Heihe River Basin. *Pearl River* **37**, 1–19. https://doi.org/10.3969/j.issn.1001-9235.2016.07.001.

Meng, X., Wang, H., Lei, X., Cai, S., Wu, H., Ji, X. & Wang, J. 2017 Hidrološko modeliranje u porječju rijeke Manas primjenom alata za procjenu tla i vode pomoću CMADS-a. *Teh. Vjesn.* **24**, 525–534. https://doi.org/10.17559/TV-20170108133334.

Meng, X., Wang, H., Shi, C., Wu, Y. & Ji, X. 2018 Establishment and evaluation of the China meteorological assimilation driving datasets for the SWAT model (CMADS). *Water (Switzerland)*. https://doi.org/10.3390/w10111555.

Meng, X., Zhang, X., Yang, M., Wang, H., Chen, J., Pan, Z. & Wu, Y. 2019 Application and evaluation of the China meteorological assimilation driving datasets For The swat model (CMADS) in poorly gauged regions in Western China. *Water (Switzerland)* **11**, 1–28. https://doi.org/10.3390/w11102171.

Mengyaun, W., Hongwei, X., Jie, Z. & Yiping, W. 2019 Runoff simulation of the Yellow River source region based on SWAT model. *J. Qinghai Univ.* **37**, 39–46. https://doi.org/10.13901/j.cnki.qhwxxbzk.2019.01.007.

Mingxing, S., Yongchao, L., Yongping, S., Hui, T., Xin, W., Chengfang, L. & Huying, M. 2018 Analyses of multiple time scales characteristics and mutation of pan evaporation variation in the source regions of the Yellow River from 1961 to 2014. *J. Glaciol. Geocryol.* **40**, 666–675. https://doi.org/10.7522/j.issn.1000-0240.2018.0072.

Mm, A., Ss, A. & Ps, B. 2019 Comparison and evaluation of gridded precipitation datasets for streamflow simulation in data scarce watersheds of Ethiopia. *J. Hydrol.* **579**, 124168.

Monteiro, J., Strauch, M., Srinivasan, R., Abbaspour, K. & Gücker, B. 2016 Accuracy of grid precipitation data for Brazil: application in river discharge modelling of the Tocantins catchment. *Hydrol. Process.* **30** (9), 1419–1430.

Moriasi, D. N., Gitau, M. W., Pai, N. & Daggupati, P. 2015 Hydrologic and water quality models: performance measures and evaluation criteria. *Trans. ASABE* **58**, 1763–1785. https://doi.org/10.13031/trans.58.10715.

Nash, J. E. & Sutcliffe, J. V. 1970 River flow forecasting through conceptual models part I – A discussion of principles – scienceDirect. *J. Hydrol.* **10**, 282–290.

Neitsch, S. L., Arnold, J. G., Kiniry, J. R., Williams, J. R. & King, K. W. 2002 *Soil and Water Assessment Tool Theoretical Documentation, Version 2000, TWRI Report TR- 191*.

Neitsch, S., Arnold, J., Kiniry, J. & Williams, J. 2011 Soil & water assessment tool theoretical documentation version 2009. *Texas Water Resour. Inst.* https://doi.org/10.1016/j.scitotenv.2015.11.063.

Poméon, T., Jackisch, D. & Diekkrüger, B. 2017 Evaluating the performance of remotely sensed and reanalysed precipitation data over West Africa using HBV light. *J. Hydrol.* https://doi.org/10.1016/j.jhydrol.2017.01.055.

Prakash, S., Mitra, A. K., Pai, D. S. & AghaKouchak, A. 2016 From TRMM to GPM: how well can heavy rainfall be detected from space? *Adv. Water Resour.* https://doi.org/10.1016/j.advwatres.2015.11.008.

Radcliffe, D. E. & Mukundan, R. 2017 PRISM vs. CFSR precipitation data effects on calibration and validation of SWAT models. *J. Am. Water Resour. Assoc.* https://doi.org/10.1111/1752-1688.12484.

Ruan, H., Zou, S., Yang, D., Wang, Y., Yin, Z., Lu, Z., Li, F. & Xu, B. 2017 Runoff simulation by SWAT model using high-resolution gridded precipitation in the upper Heihe River Basin, Northeastern Tibetan Plateau. *Water (Switzerland)* **9**, 1–23. https://doi.org/10.3390/w9110866.

Saha, S., Moorthi, S., Pan, H. L., Wu, X., Wang, J., Nadiga, S., Tripp, P., Kistler, R., Woollen, J., Behringer, D., Liu, H., Stokes, D., Grumbine, R., Gayno, G., Wang, J., Hou, Y. T., Chuang, H. Y., Juang, H. M. H., Sela, J., Iredell, M., Treadon, R., Kleist, D., Van Delst, P., Keyser, D., Derber, J., Ek, M., Meng, J., Wei, H., Yang, R., Lord, S., Van Den Dool, H., Kumar, A., Wang, W., Long, C., Chelliah, M., Xue, Y., Huang, B., Schemm, J. K., Ebisuzaki, W., Lin, R., Xie, P., Chen, M., Zhou, S., Higgins, W., Zou, C. Z., Liu, Q., Chen, Y., Han, Y., Cucurull, L. & Reynolds, R. W., Rutledge, G. & Goldberg, M. 2010 The NCEP climate forecast system reanalysis. *Bull. Am. Meteorol. Soc.* https://doi.org/10.1175/2010BAMS3001.1.

Saha, S., Moorthi, S., Wu, X., Wang, J., Nadiga, S., Tripp, P., Behringer, D., Hou, Y. T., Chuang, H. Y., Iredell, M., Ek, M., Meng, J., Yang, R., Mendez, M. P., Van Den Dool, H., Zhang, Q., Wang, W., Chen, M. & Becker, E. 2014 The NCEP climate forecast system version 2. *J. Clim.* https://doi.org/10.1175/JCLI-D-12-00823.1.

Shuai, Z., Yimin, W., Aijun, G., Kai, Z. & Ziyan, L. 2019 Influence of uncertainties in SWAT model parameters on runoff simulation in upper reaches of the Yellow River. *J. Northwest A&F Univ. (Nat. Sci. Ed)* **47**, 144–154. https://doi.org/10.13207/j.cnki.jnwafu.2019.08.018.

Song, X., Duan, Z., Kono, Y. & Wang, M. 2011 Integration of remotely sensed C factor into SWAT for modelling sediment yield. *Hydrol. Process.* https://doi.org/10.1002/hyp.8066.

Strauch, M., Bernhofer, C., Koide, S., Volk, M., Lorz, C. & Makeschin, F. 2012 Using precipitation data ensemble for uncertainty analysis in SWAT streamflow simulation. *J. Hydrol.* **414**, 413–424.

Sun, R., Yuan, H. & Yang, Y. 2018 Using multiple satellite-gauge merged precipitation products ensemble for hydrologic uncertainty analysis over the Huaihe River basin. *J. Hydrol.* https://doi.org/10.1016/j.jhydrol.2018.09.024.

Tan, M. L., Chua, V. P., Tan, K. C. & Brindha, K. 2018a Evaluation of TMPA 3b43 and NCEP-CFSR precipitation products in drought monitoring over Singapore. *Int. J. Remote Sens.* https://doi.org/10.1080/01431161.2018.1425566.

Tan, M. L., Samat, N., Chan, N. W. & Roy, R. 2018b Hydro-meteorological assessment of three GPM satellite precipitation products in the Kelantan River Basin, Malaysia. *Remote Sens.* https://doi.org/10.3390/rs10071011.

Tian, Y., Zhang, K., Xu, Y. P., Gao, X. & Wang, J. 2018 Evaluation of potential evapotranspiration based on CMADS reanalysis dataset over China. *Water (Switzerland)* **10**, 1–17. https://doi.org/10.3390/w10091126.

Tuo, Y., Duan, Z., Disse, M. & Chiogna, G. 2016 Evaluation of precipitation input for SWAT modeling in Alpine catchment: a case study in the Adige river basin (Italy). *Sci. Total Environ.* **573**, 66–82. https://doi.org/10.1016/j.scitotenv.2016.08.034.

Villarini, G., Krajewski, W. F. & Smith, J. A. 2009 New paradigm for statistical validation of satellite precipitation estimates: application to a large sample of the TMPA 0.25° 3-hourly estimates over Oklahoma. *J. Geophys. Res. Atmos.* **114**, D12106.

Wagner, P. D., Fiener, P., Wilken, F., Kumar, S. & Schneider, K. 2012 Comparison and evaluation of spatial interpolation schemes for daily rainfall in data scarce regions. *J. Hydrol.* https://doi.org/10.1016/j.jhydrol.2012.07.026.

Wang, Q., Liu, R., Men, C. & Guo, L. 2018 Application of genetic algorithm to land use optimization for non-point source pollution control based on CLUE-S and SWAT. *J. Hydrol.* https://doi.org/10.1016/j.jhydrol.2018.03.022.

Wang, N., Liu, W., Sun, F., Yao, Z., Wang, H. & Liu, W. 2020 Evaluating satellite-based and reanalysis precipitation datasets with gauge-observed data and hydrological modeling in the Xihe River Basin, China. *Atmos. Res.* **234**. https://doi.org/10.1016/j.atmosres.2019.104746.

Wei, J., Chang, J. & Chen, L. 2016 Runoff change in upper reach of Yellow River under future climate change based on VIC model. *Shuili Fadian Xuebao/Journal Hydroelectr. Eng.* **35**, 65–74. https://doi.org/10.11660/slfdxb.20160508.

Xu, Z. & He, W. 2006 Spatial and temporal characteristics and change trend of climatic elements in the headwater region of the Yellow River in recent 40 years. *Plateau Meteorology* **25**, 906–913. https://doi.org/1000-0534(2006)05-0906-08 高.

Yan, X., Jun, W., Rong, L., Xin, W. & Dongyu, J. 2019 An initial analysis of characteristics of radiation budget near ground in alpine wetland in source area of the Yellow River. *Acta Energiae Solaris Sin.* **40**, 1–10.

Yatagai, A., Kamiguchi, K., Arakawa, O., Hamada, A., Yasutomi, N. & Kitoh, A. 2012 Aphrodite constructing a long-term daily gridded precipitation dataset for Asia based on a dense network of rain gauges. *Bull. Am. Meteorol. Soc.* https://doi.org/10.1175/BAMS-D-11-00122.1.

Yu, Y. & Mu, Z. 2015 Applicability of CFSR data in runoff simulation of cold highland area. *J. Irrig. Drain.* **34**, 93–97. https://doi.org/1672-3317(2015)11-0093-05.

Yuan, F., Wang, B., Shi, C., Cui, W., Zhao, C., Liu, Y., Ren, L., Zhang, L., Zhu, Y., Chen, T., Jiang, S. & Yang, X. 2018 Evaluation of hydrological utility of IMERG final run V05 and TMPA 3b42v7 satellite precipitation products in the Yellow River source region, China. *J. Hydrol.* https://doi.org/10.1016/j.jhydrol.2018.06.045.

Zhang, P., Liu, Y., Pan, Y. & Yu, Z. 2013 Land use pattern optimization based on CLUE-S and SWAT models for agricultural non-point source pollution control. *Math. Comput. Model.* https://doi.org/10.1016/j.mcm.2011.10.061.

Zhang, L., Meng, X., Wang, H., Yang, M. & Cai, S. 2020 Investigate the applicability of CMADS and CFSR reanalysis in Northeast China. *Water (Switzerland)*. https://doi.org/10.3390/W12040996.

Zhenchun, H., Yueguan, Z., Chuanguo, Y., Jiawei, L. & Thondup, D. 2013 Effects of topography and snowmelt on hydrologic simulation in the Yellow River's source region. *Adv. Water Sci. Methodol.* **24**, 311–318. https://doi.org/10.14042/j.cnki.32.1309.2013.03.018.

Zhou, Z., Gao, X., Yang, Z., Feng, J., Meng, C. & Xu, Z. 2019 Evaluation of hydrological application of CMADS in Jinhua River Basin, China. *Water (Switzerland)*. https://doi.org/10.3390/w11010138.

Zhu, Q., Xuan, W., Liu, L. & Xu, Y. P. 2016a Evaluation and hydrological application of precipitation estimates derived from PERSIANN-CDR, TRMM 3b42v7, and NCEP-CFSR over humid regions in China. *Hydrol. Process.* **30**, 3061–3083. https://doi.org/10.1002/hyp.10846.

Zhu, Q., Xuan, W., Liu, L. & Xu, Y. P. 2016b Evaluation and hydrological application of precipitation estimates derived from PERSIANN-CDR, TRMM 3b42v7, and NCEP-CFSR over humid regions in China. *Hydrol. Process.* https://doi.org/10.1002/hyp.10846.

First received 18 February 2021; accepted in revised form 8 November 2021. Available online 22 November 2021